Low energy electron transmission through layered materials and chiral organic films

Neu, P.S.

Citation

Neu, P. S. (2024, June 12). *Low energy electron transmission through layered materials and chiral organic films*. Retrieved from https://hdl.handle.net/1887/3762501

Version:	Publisher's Version
License:	Licence agreement concerning inclusion of doctoral thesis in the Institutional Repository of the University of Leiden
Downloaded from:	https://hdl.handle.net/1887/3762501

Note: To cite this publication please use the final published version (if applicable).

5 ELECTRON TRANSMISSION AND MEAN FREE PATH IN MOLYBDENUM DISULFIDE AT ELECTRONVOLT ENERGIES

Abstract

In van der Waals (vdW) materials, the electron mean free path (MFP) is largely influenced by the discrete states in the unoccupied band structure. So far, the influence of these states has only been measured in graphene, while all measurements on other vdW materials lack energy resolution. Here, we present reflection and transmission spectra of freestanding, few-layered molybdenum disulfide (MoS_2) samples in the 0-55 eV electron range. Our measurements reveal states of enhanced electron transmissivity above the vacuum level, that correspond to the (unoccupied) density of states. We also show a full quantum mechanical calculation that confirms a good understanding of the elastic scattering in MoS_2. A model is developed to extract the inelastic MFP spectrum, which is a measure of the inelastic scattering cross section. As MoS_2 is a complicated system of different atomic planes, we expect that our methods generalize well to other van der Waals materials and heterostacks thereof.

P. S. Neu, M. Šiškins, E. E. Krasovskii, R. M. Tromp, and S. J. van der Molen, *Electron Transmission and Mean Free Path in Molybdenum Disulfide at Electron-Volt Energies*, Phys. Rev. B **107**, 075427 (2023).

5.1 Introduction

The electron mean free path (MFP) is a material-specific quantity, describing the decay length of an electron beam through a material at a specific electron energy. Especially the MFP of low-energy electrons is important, as it affects the probing depth and damage in scanning electron microscopy (SEM) as well as the exposure of resists in electron beam lithography. While the mean free path of electrons through bulk solids has been researched for more than a century, it has barely been studied in the comparably new class of van der Waals materials. Moreover, subtle energy-dependent features, intimately related to the unoccupied electron band structure, have generally been missed due to a lack of energy and momentum resolution.

For many different solids, the electron MFP has been measured over a large energy range and determined to roughly follow the same U-shape curve, the so-called universal curve [1], which has a minimum around 30 eV, but is otherwise featureless. Fewer reports are available for layered materials, especially in the low-energy range. For graphene, the most popular van der Waals material, the low-energy MFP has been reported to be in the order of a few layers based on Electron Energy Loss Spectroscopy (EELS) [2], measurements of the secondary electron spectrum generated in a SEM [3] and by photoemission [4]. Recently, our group has demonstrated a more direct method to extract the MFP from a combination of low energy electron microscopy (LEEM) and electron Volt-transmission electron microscopy (eV-TEM) [5,6]. In contrast to the 'universal' curve, our study on few-layer graphene showed multiple maxima and minima depending on layer count. These features are related to (unoccupied) interlayer electron bands that are typical of van der Waals materials. For the case of graphene, these can be understood within a relatively simple model of Fabry-Pérot-like electron interference between the consecutive layers, leading to well-defined electron transmission resonances [7–10].

In this contribution, we use this new methodology, i.e., the combination of LEEM and eV-TEM, to study MoS_2, a member of a more complicated and diverse group of two-dimensional materials: the transition metal dichalcogenides (TMDs). The different TMDs are closely related in crystallographic structure, every layer consisting of a plane of transition metal atoms sandwiched between two chalcogen atom (S, Se, Te) planes. However, TMDs show significant variation in their electric properties. Molybdenum disulfide (MoS_2) is a promising TMD, having a band gap in the visible to IR range, making it suitable for photovoltaic applications. Remarkably, the band gap is indirect for multilayer MoS_2, whereas it becomes direct for monolayer MoS_2. The chemical and semiconducting properties of MoS_2 make it a popular substrate for (high-energy) TEM analyses of catalysis [11, 13–16]. The only low-energy transmissivity measurements reported so far have been performed with the 'virtual substrate' method [26], i.e., by secondary electrons emitted from underlying substrates.

5.2 Experiment

Here we report and analyze electron reflectivity and transmissivity spectra of the 2H polytype of MoS_2 in the low energy (0 - 55 eV) range, obtained by LEEM and eV-TEM. We demonstrate that the energy dependent structure observed is convincingly explained from the distribution of unoccupied electron states above the vacuum energy. From the combination of these reflection

and transmission spectra, we deduce unique information on the elastic and inelastic scattering electron path lengths within MoS_2 vs. energy.

For our experiments, a thin flake of exfoliated MoS_2 (2H polytype) was transferred using the all-dry viscoelastic method [11] onto a silicon nitride TEM grid (PELCO® Holey Silicon Nitride, 2.5 um holes (optical images in the supplemental information [12], Fig. 5.S1) that had been sputter-coated with 5 nm Pt/Pd to improve conductivity. The sample was gently annealed by laser heating (808 nm, 10.7 W, approx. 300° C) in the UHV sample chamber of the LEEM instrument. In aberration-corrected LEEM mode [13] we image the sample using low energy electrons specularly reflected from the sample (see sketch in Fig. 5.1c). For eV-TEM, we use a second electron source behind the sample to form transmission images of low energy electrons transmitted without scattering and/or energy loss [5,6]. As both methods are available in the same instrument, we can image the same sample area in both reflectivity and transmissivity, so that they can be readily and directly compared. To illustrate this, a transmission image (eV-TEM) of MoS_2 on the holey SiN is shown in Fig. 5.1a. In Fig. 5.1b, we show the same image, but with a reflection (LEEM) image pasted on top of the eV-TEM image, so as to demonstrate its position. To obtain detailed spectral information, we scan the energy of the electrons incident on the sample in the range from 0 to 55 eV in steps of 0.1 eV and record images in both transmission and reflection at each energy. The energy resolution of the spectra is limited by the energy spread of the respective electron guns, i.e., 0.3 eV for the cold field emission gun in LEEM and 0.8 eV for the thermal Barium Oxide emitter in eV-TEM. Note that in both LEEM and eV-TEM a contrast aperture in the diffraction plane has been inserted around the specular spot, so contributions of inelastically and/or diffusely scattered electrons and higher order diffraction spots are blocked.

5.3 Results

The eV-TEM image, Fig. 5.1a, shows three different layer counts in the flake. (Note that the 50 nm thick TEM grid support is fully blocking the low-energy electrons outside the holey structure). While the thinnest area of the flake is most transmissive, the area on the left edge is not transmissive enough to allow distinguishing the holes in the underlying grid. Throughout the whole energy range the thinnest part is most transmissive and the thickest part is least transmissive, which is as one may expect in a system dominated by inelastic scattering. The LEEM image in Fig. 5.1b shows some contamination of the sample, supposedly with residues from the preparation process. These contaminants cluster together upon the first illumination with the electron beam, which is common for polycarbonate residues from the exfoliation and stamping process. It stands out that the areas of lower layer count are less contaminated, which indicates that either the sticking coefficient is lower on these surfaces or that the contaminants diffused in between layers. Averaged over the area of one covered hole, the contaminants reduce the reflected intensity by ~25% throughout the considered energy range compared to small pristine areas.

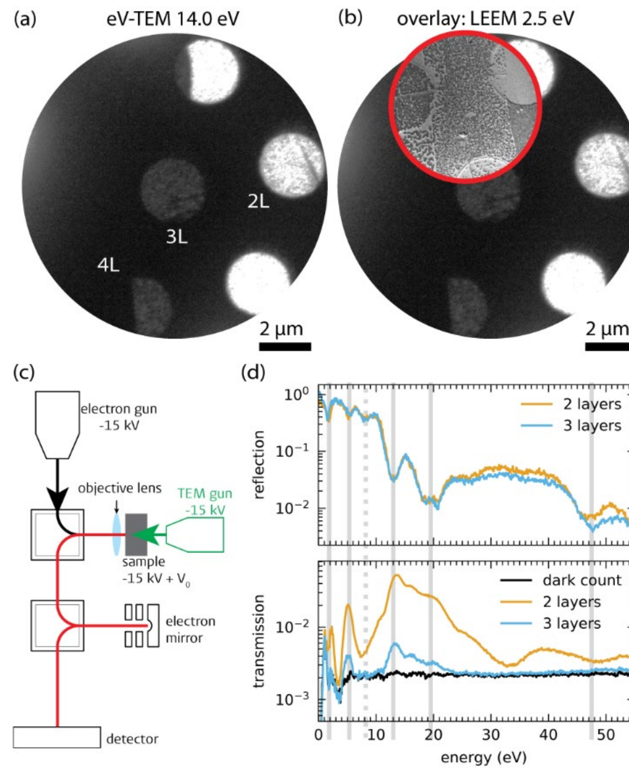

Figure 5.1: (a) eV-TEM image of 2, 3 and 4 layer (labeled 2L, 3L and 4L) MoS_2 flake covering a grid of holes, acquired by transmitted low-energy electrons. In (b), a smaller scale reflection image (LEEM) is shown, placed on top of the transmission image in (a) to pinpoint its position. (c) shows the low energy electron microscope (LEEM) setup with the additional electron gun behind the sample used for eV-TEM. (d) Reflection and transmission spectra of the bi- and trilayer areas. The lines mark the minima in reflectivity, i.e., states above the vacuum level where one expects corresponding transmission maxima at the same energy.

The reflection and transmission data sets of images recorded at 0-55 eV allow us to select areas of a specific layer count and extract the corresponding spectra. We have chosen flat, freestanding areas and for each energy have averaged over a circular area that almost fills a TEM grid hole. Figure 5.1d displays the spectra obtained, which have all been normalized to the incoming electron flux. For completeness, Figure 5.1d also displays the dark count (DC), which was extracted from an area on the TEM grid support blocking all electrons. The transmission spectrum of the four-layer area is not shown, as it is not distinguishable from the dark count. The dark count is caused by the microchannel plate used to amplify the electron signal: bright features, here predominantly the uncovered TEM grid holes, will ‘bleed’ into the adjacent detector area. The apparent features in the dark count spectrum are thus an artifact of the automatic adaptive gain of the channel plate [14] that prevents overexposure of the brightest features in the image. For the analysis following, we therefore subtracted the energy-dependent dark count from the transmission spectra.

In Fig. 5.1d, a set of characteristic reflectivity minima are shown, marked by vertical lines. Their positions are consistent with previous reports on MoS_2 [15,16]. Furthermore, they are consistent with calculations of the projected Density of (unoccupied) States (pDOS, [12] Fig. 5.S2): The projected bands at the Γ point, i.e., at zero in-plane momentum, coincide with the

reflection minima (transmission maxima) at the same energy. Indeed, an incoming electron resonant with an unoccupied state has a strongly enhanced probability of propagating into the material, leading to a minimum in reflectivity, and a maximum in transmission. In general, the electron reflectivity will thus depend on the dispersion of the states, i.e. on their energy vs. in-plane k-vector, as given by the pDOS and as demonstrated by recent angle-resolved reflected-electron spectroscopy (ARRES) [10]. In the LEEM and eV-TEM experiments reported here, the electrons are incident and detected exclusively along the surface normal, thus probing the electronic band structure at the Γ point only. (Off-normal reflected/transmitted electrons are filtered out by the contrast aperture.)

Of special importance is that all reflectance spectra recorded show a dip around 5.4 eV. This dip is absent in monolayer MoS_2, as calculations and previous experiments [15] show (see also below). We conclude that all areas of the sample are at least 2 layers thick, although we had optically preselected the thinnest MoS_2 flakes during sample preparation. Whereas the study in reference [15] could only probe the electron reflectivity, the current study also employs eV-TEM to measure the transmissivity of the same sample area. The high transmissivity of the thinnest area strongly suggests that we are looking at 2, 3 and 4 layers of MoS_2.

Let us now look at Fig. 5.1d in more detail. It shows a rather broad window of maximum transmissivity at a remarkably high energy range, i.e., from 10 to 25 eV. This feature is in sharp contrast to the simple case of graphene where the highest transmissivity is below 5 eV. We will discuss this phenomenon in more detail below. Furthermore, Fig. 5.1d shows that the maxima in transmission align with the minima in reflection, as illustrated by the vertical lines. This is exactly what a simple resonant theory, in which atomic layers act as 'semi-transparent' mirrors would yield: at resonance, there will be constructive interference for forward propagation (transmission) and destructive interference in backward propagation [5]. However, such a simple model will not suffice here as it cannot explain all features. The reflection maximum at 10 eV, for example, comes with a shoulder in transmission, on the flank of some broader feature. Furthermore, the reflection minimum at 8.2 eV (dashed vertical line) has no corresponding feature in transmission. We will attribute the latter to strong inelastic scattering at this particular energy (see below).

To gain further insight into the nature of the electron reflection and transmission, we calculated electron scattering by 1, 2 and 3 layers of MoS_2 using the *ab initio* method based on Bloch-waves developed in ref. [17]. Its application to an isolated slab is described in ref. [18]: In the scattering region the wave function is a linear combination of the eigenfunctions of an auxiliary three-dimensional periodic crystal, which contains the TMD sandwich as part of the unit cell. The Bloch eigenfunctions of the auxiliary crystal are obtained in terms of augmented plane waves, see refs. [17,18]. Inelastic scattering was taken into account by the optical potential, which increases smoothly with energy as calculated for the similar TMD, tungsten diselenide (WSe_2), in ref. [19] within the *GW* approximation based on a full energy and momentum dependent *ab initio* dielectric function of WSe_2.

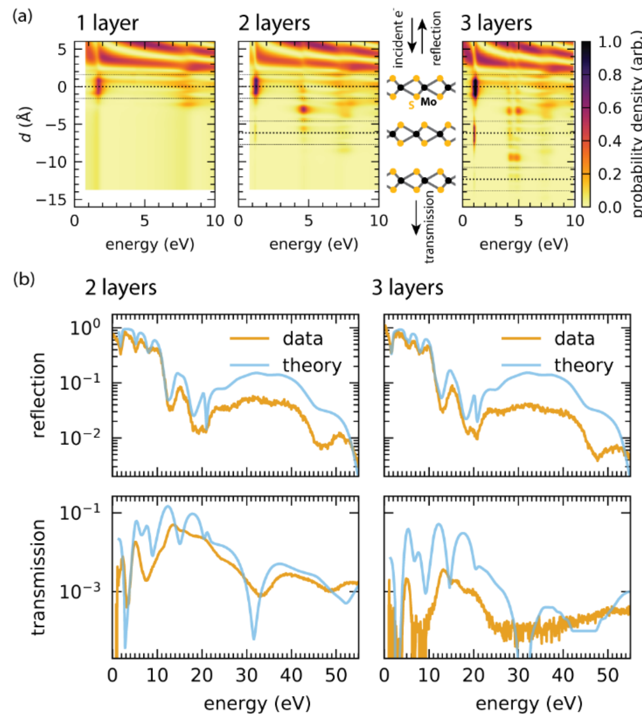

Figure 5.2: (a) Calculated probability density along the out-of-plane direction for an electron wave incident from the top for 1, 2 and 3 layers of MoS_2, with the Mo and S planes marked as dotted lines. (b) Comparison of the recorded reflection and transmission (dark count subtracted) spectra and the calculated values. The features of the reflection curves match well. The experimental transmission spectrum appears more broadened as discussed in the text.

Figure 5.2a shows the solution to the scattering problem for an electron plane wave that is at normal incidence on the layers of MoS_2 from the top side and is partially reflected and partially transmitted. Note that it is the electron probability density that is plotted. Inside the material, the electron density shows where the electronic states are localized, whereas on the top vacuum side we see the interference of the incoming wave with the reflected wave. The electron wavelength in vacuum shortens with increased energy, as is seen in the interference between the incoming and reflected wave in front of the material.

Let us next focus on the (unoccupied) states involved (see Fig. 5.2a). The resonance at 1 eV has its highest electron density within the layers, while the resonance at 4 - 5 eV, which is characteristic of the multilayer (n>1, absent in the monolayer), is centered between the layers. This interlayer resonance, around 4.5 eV for the bilayer, splits into two resonances for the trilayer, in theory causing a splitting of the reflection minimum as in graphene, but that is beyond the spectral resolution of our measurement. The electron density is not symmetrical but shifted towards the side of the incoming electrons. For example, the state at 1 eV has most of the electron density centered around the first layer, and it considerably decreases towards the second or even the third layer. Similarly, in the 3-layer case the interlayer state at 4 - 5 eV has a higher electron density between the first and second layer than between the second and third layer. The fact that the electron density is shifted towards the side of the incoming electrons intuitively explains why the reflection spectra of two and three layer MoS_2 largely coincide.

We note that the reflectivity and transmissivity spectra shown in Figure 5.2b are calculated for the specular beam. This was done to make them comparable to the measurement, where a diffraction-space aperture was placed around the (0,0) beam. To mimic the resolution of our instrument, the theoretical spectra were broadened by a Gaussian function with a FWHM of 0.3 eV and 0.8 eV for LEEM and eV-TEM, respectively. For the reflectivities, the measured features match the calculations very well. The fact that the measured reflectivity is lower than calculated is at least in part caused by the contaminants discussed above.

For the transmissivity spectra the calculated and measured spectra show qualitative correspondence, although there are clear differences. For example, the transmission intensity measured is generally lower than predicted by calculation, although still of the same magnitude. We relate this to contamination on the sample surface. In general, the energies of the transmission maxima and minima in experiment and theory match rather well, although the peaks and dips are less pronounced in the experiment. For example, the sharp minimum and maximum at a few eV as well as the large window of enhanced transmissivity from 10 eV to 25 eV reproduce for both the bilayer and the trilayer. But there is a clear outlier: a transmission maximum at 8 eV is calculated but not observed. This peak may be suppressed by inelastic loss processes [20,21]. The dip in reflectivity is less affected by inelastic loss, as neither electrons that are transmitted elastically nor electrons that scatter inelastically contribute to the reflectivity.

The LEEM-IV and eV-TEM spectra broaden with increasing energy, an effect that has also been observed for multilayer graphene [7,22]. We relate this to an increased loss in each layer, comparable to how the finesse in a Fabry-Pérot resonator [23] decreases when the reflectivity of the mirrors goes down. As the lifetime of an electron in an unoccupied state decreases, the spectral features broaden. These losses could be due to inelastic scattering, that generally increases with energy as more scattering paths become available, or due to increased elastic scattering out of the aperture. Note that increasing loss effects as a function of energy are also incorporated in our first principles calculations via an energy-dependent optical potential.

As introduced above, the transverse electron mean free path of graphene has been determined by direct [5] and more indirect methods, like photoemission [4], TOF of secondary electrons [24] and deconvolution of EELS spectrum [2]. Although the effects of multiple scattering increase the MFP if one also counts the distance travelled within the zig-zag path [25], in the case of MoS_2 the transmissivity is so low that we can make the approximation to neglect multiple scattering. This leads to the following simple model. Let us define R(E) as the fraction of electrons reflected at an energy E. Then 1-R(E) is the percentage of electrons travelling into the material. The share of electrons that are actually transmitted through the material, T(E), is then equal to (1-R(E)) attenuated by the losses within the film due to scattering within the two or three layers of MoS_2, respectively. With the thickness d (in layers), the transmissivity can hence be written as:

$$\mathrm{T(E)} = \left(1 - \mathrm{R(E)}\right) \cdot \exp\left(-\mathrm{d}/\lambda(\mathrm{E})\right) \qquad (1)$$

where λ(E) is the energy-dependent (inelastic) electron MFP. Note that the reflectivity R(E) in this model is independent of layer count. This is justified by the reflection data shown in Fig.

5.1d. Applying this model for d=2 layers, we obtain the MFP vs. energy curve shown in Figure 5.3a, which is between 0.3 and 0.7 layers, or 1.8 Å to 4.3 Å.

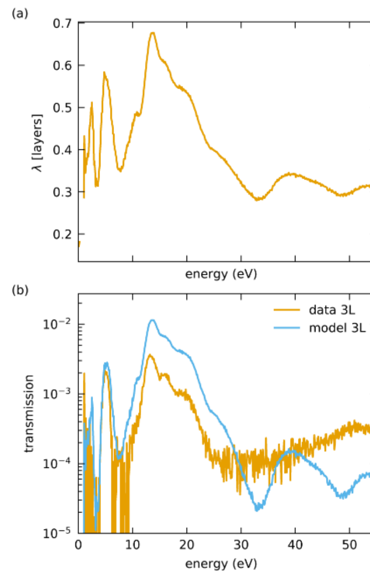

Figure 5.3: (a) From the reflectivity and transmissivity observed in the 2 layer data, we calculate the mean free path $\boldsymbol{\lambda}$. Using the extracted $\boldsymbol{\lambda}$ in a simple model to predict the transmissivity (b) of the 3 layer sample yields reasonable agreement with the measured spectra.

To check for consistency, we take the λ(E) function obtained for the 2-layer case and calculate what should come out for the 3-layer case. In other words, we insert λ(E) back into eq. 1, together with the 3 layer R(E) function, and subsequently set d to 3 layers. The transmissivity function calculated this way (Fig. 5.3b) follows the measured one quite well up to an energy of 25 eV. At higher energies the transmissivity is somewhat lower for the 3-layer data (until the noise of 10^{-4} dominates the spectrum). We relate this to the somewhat higher contamination observed on the surface of the trilayer.

5.4 Discussion

Next, we compare our data to the measurements of low-energy MFP by Da et al. [26] who employ the 'virtual substrate' method. They report significantly larger MFP values of 15 – 30 Å for bilayer MoS_2 ([12], Fig. 5.S3). Accordingly, they also report a larger transmissivity of 45% - 60%. We propose that this significant difference of an order of magnitude is inherent to the different measurement techniques: In the virtual substrate method, the incident electrons, i.e., the secondary electrons emitted from the virtual substrate, are non-directional, so even after diffuse and/or inelastic scattering they contribute to the measured signal. In contrast, in our eV-TEM method, a collimated beam of electrons is incident on the sample, and measures have been taken to filter out all electrons that have been scattered diffusely and/or inelastically. The contamination of the sample discussed above only has a minor effect, since assuming a 25% higher value for T(E) increases the calculated MFP by less than 1 Å.

Da et al. also report a large window of increased MFP at 7-50 eV. This would correspond to what we see in the range 8-50 eV in Fig. 5.3a, if one were to consider that the dip in MFP

around 32 eV is not visible in their data due to a decreasing signal-to-noise ratio. Also, the MFP maxima at 2.3 eV and 5 eV cannot be distinguished in their measurements, which may be related to the lack of collimation of the secondary electron probe beam. Importantly, the unoccupied bands have a dispersion depending on electron momentum, which will further blur the features [9]. Hence, from the experimental side there are differences in methodology and hence in measurement resolution.

5.5 Summary

To summarize, we have studied electron transmission through MoS_2 and have directly obtained the mean free path as a function of electron energy, λ(E), in the 0-55 eV energy range. This demonstrates that we can extend the methodology we previously applied to graphene [5,6] to the more complex TMDs. In contrast to graphene, the maximum transmissivity is found in a large window at 10-25 eV, rather than at energies below 5 eV. As for graphene, the transmission maxima found experimentally can be related to (resonant) electronic states within the MoS_2, as obtained by calculations. However, in a more complicated system such as MoS_2, these states are not limited to simple interlayer resonances. Note that in contrast to EELS, which measures the strength of inelastic scattering as a function of energy loss, the inelastic mean free path extracted here is a direct measure of the energy-dependent scattering cross section as a function of initial electron energy.

Having demonstrated our methodology for a rather complex system such as MoS_2, we expect our methods and understanding to generalize to the other transition metal dichalcogenides and to heterostacks of van der Waals materials. In all cases, unoccupied electron states will play a large role in electron propagation and mean free paths.

Acknowledgements

We acknowledge Herre van der Zant, Andres Castellanos-Gomez, Peter Steeneken and Martin Lee for support in preparing the samples. This research was funded by the Spanish Ministry of Science, Innovation and Universities (EK, Project No. PID2019-105488GB-I00) and the Dutch Research Council (PN, NWO Vrije Programma TNW18.071).

Appendix

Optical Images

Optical micrographs of the sample are shown in Figure 5.A1. All measurements reported in the main text were performed on the thin part of the MoS_2 flake, here towards the top of the image. Also, the TEM grid holes underneath the flake and another thicker MoS_2 flake to the right are visible.

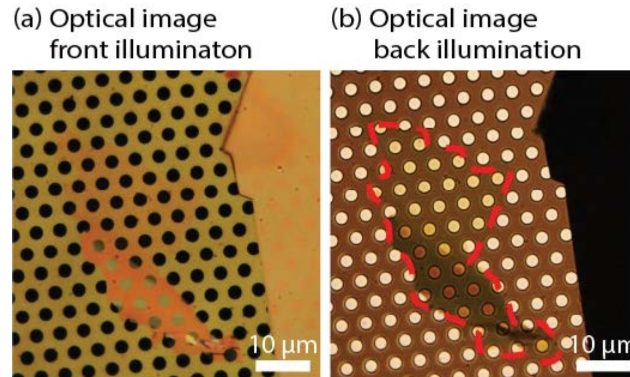

Figure 5.A1: Optical images after stamping the MoS_2 flake to the holey support grid. The flake is digitally outlined in the back illumination micrograph (b).

Projected Density of States

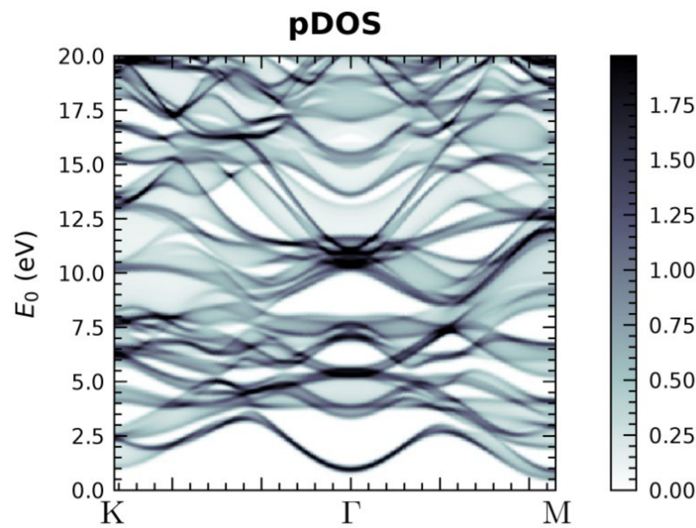

Figure 5.A2: Calculated projected Density of States (pDOS) of bulk MoS_2. The energy 0 eV corresponds to the vacuum level.

The density of states (DOS) above the vacuum level is calculated and projected along the out-of-plane direction in Figure 5.A2. The LEEM and eV-TEM experiments reported in the main text probe the band structure at the Γ point, as only electrons at perpendicular incidence and perpendicular reflection/transmission are measured.

Mean Free Path: comparing with previous work

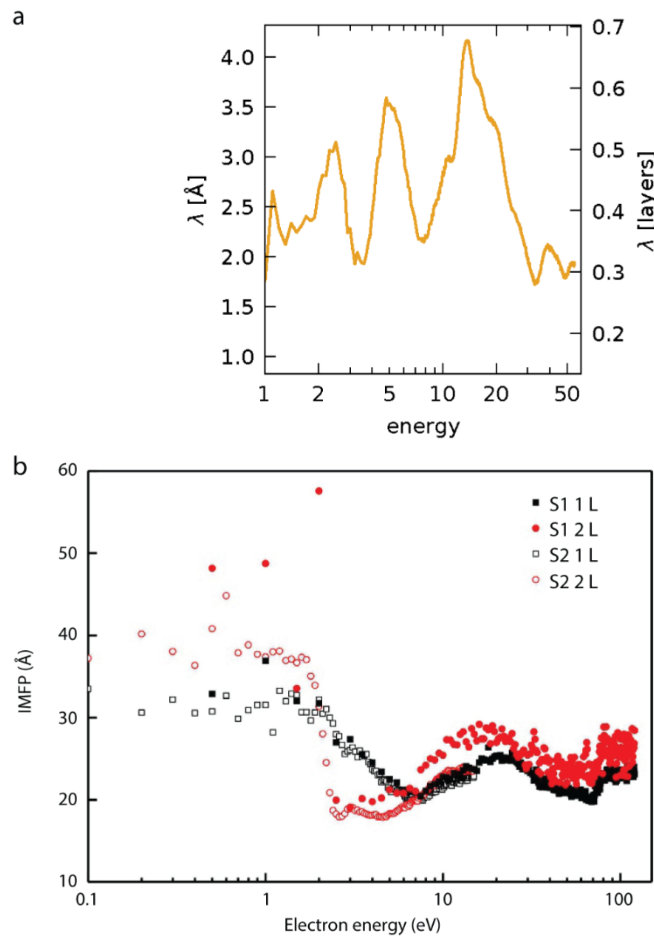

Figure 5.A3: Inelastic Mean Free Paths (IMFP) obtained (a) from the combination of LEEM and eV-TEM measurements (main text, eq. 1) compared to (b) results obtained by Da et al. by the virtual substrate method. Plot (b) is reproduced from [26].

Both methods of obtaining the IMFPs yield comparable key features in bilayer MoS_2 (Fig. 5.A3, a, red curves in b). Foremost, the broad IMFP maximum from 8 – 30 eV is reproduced in both methods. Also, the maximum at 5 eV in (a) may be visible in measurement S1 2L (b).

The most striking difference is the scale of the IMFPs obtained: 2 - 4 Å in our experiment and 15 - 30 Å reported by Da et al. This may be explained by the different momentum distributions of the electrons used in the two experiments: While the electrons in our experiment have close to zero in-plane momentum (with respect to the sample) when entering and exiting the material, the photoelectrons used in the virtual substrate method have a broad distribution of in-plane momenta when incident on the MoS_2 and also when measured after transmission. That means that in the virtual substrate method scattering events that change the in-plane momentum of the electrons don't contribute to lowering the IMFP. The broad distribution of in-plane momenta in the virtual substrate method also explains its apparently lower resolution: The electrons probe the band structure averaged over a large part of reciprocal space (see the pDOS, Figure 5.A2), thus the discrete states at the Γ point shown in (a) appear broadened.

References

[1] M.P. Seah, W.A. Dench, Quantitative electron spectroscopy of surfaces: A standard data base for electron inelastic mean free paths in solids, Surf. Interface Anal. 1 (1979) 2–11. https://doi.org/10.1002/sia.740010103.

[2] W.S.M. Werner, A. Bellissimo, R. Leber, A. Ashraf, S. Segui, Reflection electron energy loss spectrum of single layer graphene measured on a graphite substrate, Surf. Sci. 635 (2015) L1–L3. https://doi.org/10.1016/j.susc.2014.12.016.

[3] O.Y. Ridzel, V. Astašauskas, W.S.M. Werner, Low energy (1–100 eV) electron inelastic mean free path (IMFP) values determined from analysis of secondary electron yields (SEY) in the incident energy range of 0.1–10 keV, J. Electron Spectros. Relat. Phenomena 241 (2020) 146824. https://doi.org/10.1016/j.elspec.2019.02.003.

[4] A. Locatelli, G. Zamborlini, T.O. Menteş, Growth of single and multi-layer graphene on Ir(100), Carbon N. Y. 74 (2014) 237–248. https://doi.org/10.1016/j.carbon.2014.03.028.

[5] D. Geelen, J. Jobst, E.E. Krasovskii, S.J. van der Molen, R.M. Tromp, Nonuniversal Transverse Electron Mean Free Path through Few-layer Graphene, Phys. Rev. Lett. 123 (2019) 086802. https://doi.org/10.1103/PhysRevLett.123.086802.

[6] P.S. Neu, D. Geelen, A. Thete, R.M. Tromp, S.J. van der Molen, Complementary LEEM and eV-TEM for imaging and spectroscopy, Ultramicroscopy 222 (2021) 113199. https://doi.org/10.1016/j.ultramic.2020.113199.

[7] H. Hibino, H. Kageshima, F. Maeda, M. Nagase, Y. Kobayashi, Y. Kobayashi, H. Yamaguchi, Thickness Determination of Graphene Layers Formed on SiC Using Low-Energy Electron Microscopy, E-Journal Surf. Sci. Nanotechnol. 6 (2008) 107–110. https://doi.org/10.1380/ejssnt.2008.107.

[8] R.M. Feenstra, M. Widom, Low-energy electron reflectivity from graphene: First-principles computations and approximate models, Ultramicroscopy 130 (2013) 101–108. https://doi.org/10.1016/j.ultramic.2013.02.011.

[9] J. Jobst, J. Kautz, D. Geelen, R.M. Tromp, S.J. van der Molen, Nanoscale measurements of unoccupied band dispersion in few-layer graphene, Nat. Commun. 6 (2015) 8926. https://doi.org/10.1038/ncomms9926.

[10] J. Jobst, A.J.H. van der Torren, E.E. Krasovskii, J. Balgley, C.R. Dean, R.M. Tromp, S.J. van der Molen, Quantifying electronic band interactions in van der Waals materials using angle-resolved reflected-electron spectroscopy, Nat. Commun. 7 (2016) 13621. https://doi.org/10.1038/ncomms13621.

[11] A. Castellanos-Gomez, M. Buscema, R. Molenaar, V. Singh, L. Janssen, H.S.J. van der Zant, G.A. Steele, Deterministic transfer of two-dimensional materials by all-dry viscoelastic stamping, 2D Mater. 1 (2014) 011002. https://doi.org/10.1088/2053-1583/1/1/011002.

[12] See Appendix for optical images, the calculated projected Density of States and the mean free path compared to previous experimental work.

[13] R.M. Tromp, J.B. Hannon, A.W. Ellis, W. Wan, A. Berghaus, O. Schaff, A new aberration-corrected, energy-filtered LEEM/PEEM instrument. I. Principles and design, Ultramicroscopy 110 (2010) 852–861. https://doi.org/10.1016/j.ultramic.2010.03.005.

[14] T.A. de Jong, D.N.L. Kok, A.J.H. van der Torren, H. Schopmans, R.M. Tromp, S.J. van der Molen, J. Jobst, Quantitative analysis of spectroscopic low energy electron microscopy data: High-dynamic range imaging, drift correction and cluster analysis, Ultramicroscopy 213 (2020) 112913. https://doi.org/10.1016/j.ultramic.2019.112913.

[15] T.A. de Jong, J. Jobst, H. Yoo, E.E. Krasovskii, P. Kim, S.J. van der Molen, Measuring the Local Twist Angle and Layer Arrangement in Van der Waals Heterostructures, Phys. Status Solidi 255 (2018) 1800191. https://doi.org/10.1002/pssb.201800191.

[16] Z. Dai, W. Jin, M. Grady, J.T. Sadowski, J.I. Dadap, R.M. Osgood, K. Pohl, Surface structure of bulk 2H-MoS2(0001) and exfoliated suspended monolayer MoS2: A selected area low energy electron diffraction study, Surf. Sci. 660 (2017) 16–21. https://doi.org/10.1016/j.susc.2017.02.005.

[17] E.E. Krasovskii, Augmented-plane-wave approach to scattering of Bloch electrons by an interface, Phys. Rev. B 70 (2004) 245322. https://doi.org/10.1103/PhysRevB.70.245322.

[18] E. Krasovskii, Ab Initio Theory of Photoemission from Graphene, Nanomaterials 11 (2021) 1212. https://doi.org/10.3390/nano11051212.

[19] F. Siek, S. Neb, P. Bartz, M. Hensen, C. Strüber, S. Fiechter, M. Torrent-Sucarrat, V.M. Silkin, E.E. Krasovskii, N.M. Kabachnik, S. Fritzsche, R.D. Muiño, P.M. Echenique, A.K. Kazansky, N. Müller, W. Pfeiffer, U. Heinzmann, Angular momentum–induced delays in solid-state photoemission enhanced by intra-atomic interactions, Science 357 (2017) 1274–1277. https://doi.org/10.1126/science.aam9598.

[20] H.C. Nerl, K.T. Winther, F.S. Hage, K.S. Thygesen, L. Houben, C. Backes, J.N. Coleman, Q.M. Ramasse, V. Nicolosi, Probing the local nature of excitons and plasmons in few-layer MoS2, NPJ 2D Mater. Appl. 1 (2017) 1–8. https://doi.org/10.1038/s41699-017-0003-9.

[21] E. Moynihan, S. Rost, E. O’connell, Q. Ramasse, C. Friedrich, U. Bangert, Plasmons in MoS2 studied via experimental and theoretical correlation of energy loss spectra, J. Microsc. 279 (2020) 256–264. https://doi.org/10.1111/jmi.12900.

[22] D. Geelen, eV-TEM: Transmission Electron Microscopy with Few-eV Electrons, Doctoral dissertation, Leiden University, 2018. http://hdl.handle.net/1887/63484.

[23] N. Ismail, C.C. Kores, D. Geskus, M. Pollnau, Fabry-Pérot resonator: spectral line shapes, generic and related Airy distributions, linewidths, finesses, and performance at low or frequency-dependent reflectivity, Opt. Express 24 (2016) 16366–16389. https://doi.org/10.1364/OE.24.016366.

[24] I. Konvalina, B. Daniel, M. Zouhar, A. Paták, I. Müllerová, L. Frank, J. Piňos, L. Průcha, T. Radlička, W.S.M. Werner, E.M. Mikmeková, Low-Energy Electron Inelastic Mean Free Path of Graphene Measured by a Time-of-Flight Spectrometer, Nanomaterials 11 (2021) 2435. https://doi.org/10.3390/nano11092435.

[25] L.H. Yang, B. Da, H. Yoshikawa, S. Tanuma, J. Hu, J.W. Liu, D.M. Tang, Z.J. Ding, Low-energy electron inelastic mean free path and elastic mean free path of graphene, Appl. Phys. Lett. 118 (2021) 053104. https://doi.org/10.1063/5.0029133.

[26] B. Da, J. Liu, M. Yamamoto, Y. Ueda, K. Watanabe, N.T. Cuong, S. Li, K. Tsukagoshi, H. Yoshikawa, H. Iwai, S. Tanuma, H. Guo, Z. Gao, X. Sun, Z. Ding, Virtual substrate method for nanomaterials characterization, Nat. Commun. 8 (2017) 15629. https://doi.org/10.1038/ncomms15629.